Hybrid Approach to Conduct Failure Prognostics of Automotive Electronic Control Unit Using Stress Sensor as *In Situ* Load Counter

Bulong Wu, Dae-Suk Kim, Bongtae Han, Alicja Palczynska, Alexandru Prisacaru, and Przemyslaw Jakub Gromala

***Abstract*— A model/sensor hybrid approach is implemented to conduct failure prognostics of an automotive electronic control unit (ECU). A 3-D finite-element model simulating a complex ECU is built, and its predictability is calibrated and verified by an optical displacement measurement technique called moiré interferometry. On the sensor front, a silicon-based piezoresistive stress sensor is embedded into the ECU to provide *in situ* stress measurements during operations. A stress metric is defined using the stress values of 12 cells in each sensor, and it is converted to *in situ* loading histories using the calibrated finite-element model. The modeling and verification steps that lead to the predictive finite-element model are described. The proposed hybrid approach is implemented using the data obtained from a molded ECU subjected to thermal cycling conditions, and the forces at an interface between an aluminum wire bond and metal pad are investigated.**

***Index Terms*— Electronic control unit (ECU), finite-element analysis (FEA) modeling, load counter, model verification, moiré interferometry, stress sensor.**

I. Introduction

IT IS expected that advanced electronic components and smart systems would dictate the level of innovations in nearly all industrial sectors, including automotive and other transport/logistics solutions, production equipment, and energy and other infrastructure. In particular, more and more advanced electronics have been adopted in automotive technologies to enhance user interfaces.

One such component is an automotive electronic control unit (ECU), which is an embedded system that controls an electrical system or subsystems in a transport vehicle. Typical applications include engine control, power control, and transmission control. ECU performance is directly related to: 1) on-road performance; 2) fuel consumption; 3) exhaust gas reduction; and 4) extended battery life. Connectivity and automation for autonomous vehicle technology will require significant changes in existing ECU technologies.

In a conventional ECU, a protective metal case has been used to ensure reliability under harsh environmental conditions. Recently, an epoxy molding compound (EMC) was adopted to replace the metal case. The EMC technology reduced the manufacturing cost significantly, yet the presence of a large amount of outer EMC increased the stresses of ECUs during the transfer molding process and operations [1]–[3]. Reliability of ECU is directly related to automobile safety. The long-term reliability of this newly adopted manufacturing technology should be assessed to make the technology a more viable alternative to various ECUs.

A piezoresistive stress sensor was developed to measure directly the stresses of a silicon chip embedded in a package. The sensor was implemented successfully to investigate the effect of encapsulation process on the package stress [4] and to monitor the wire-bonding process [5]. The sensor was also considered for prognostics and health management [6]. In [6], the changes in stresses measured by the sensor were observed before delamination occurred, which could be used as a signal for failure.

Numerical modeling such as finite-element analysis (FEA) can be calibrated and subsequently utilized to predict the thermally induced deformations of the critical parts in molded ECUs. However, accurate assessment of the deformations under automotive driving conditions is challenging because the operating environments of ECU vary significantly with users and locations. It is important to document the *in situ* loading condition to conduct failure prognostics realistically. The piezoresistive stress sensor has a unique advantage over other deformation measurement techniques; it can provide *in situ* stress measurements during operations. This advantage can be further utilized to count actual loading conditions.

In this paper, a 3-D finite-element model simulating a complex ECU is built, and its predictability is examined and calibrated by an optical displacement measurement technique called moiré interferometry. The calibrated model and the load count obtained from the stress sensor provide a hybrid approach to conduct failure prognostics of molded ECUs. The modeling construction and a detailed procedure to calibrate the model are presented after briefly describing two experimental techniques. Then, the proposed hybrid approach is presented

Manuscript received December 4, 2017; revised February 25, 2018; accepted March 10, 2018. Date of publication April 5, 2018; date of current version January 17, 2019. Recommended for publication by Associate Editor J.-H. Zhao upon evaluation of reviewers' comments. *(Corresponding author: Bongtae Han.)*

B. Wu, D.-S. Kim, and B. Han are with the Mechanical Engineering Department, University of Maryland at College Park, College Park, MD 20742 USA (e-mail: bthan@umd.edu).

A. Palczynska, A. Prisacaru, and P. J. Gromala are with Robert Bosch GmbH, 72703 Reutlingen, Germany.

Color versions of one or more of the figures in this paper are available online at http://ieeexplore.ieee.org.

Digital Object Identifier 10.1109/TCPMT.2018.2815633

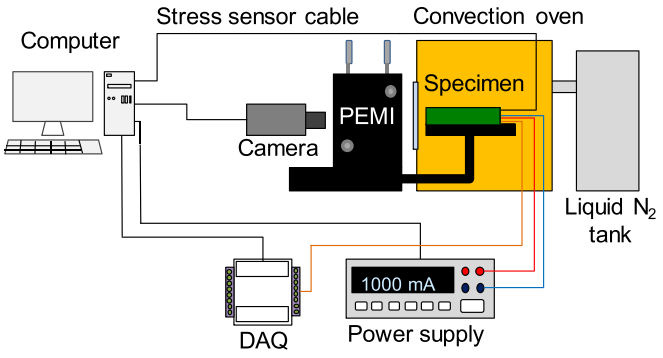

Fig. 1. Schematic of the experimental system for displacement measurements.

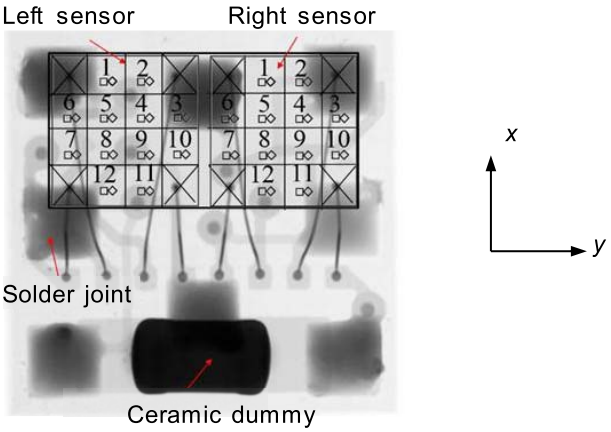

Fig. 2. X-ray image of LGA sensor package.

using the data obtained from the molded ECUs subjected to thermal cycling conditions.

II. Background: Experimental Techniques

A. Moiré Interferometry

Moiré interferometry maps the deformations of advanced engineering structures with extremely high resolution. It has been used extensively for the thermal deformation analyses of various semiconductor packages [7]–[15]. In this method, a high-frequency cross-line grating is replicated on a specimen cross section, and it deforms together with the specimen. A pair of collimated beams of laser light strikes the specimen and a portion is diffracted back, perpendicular to the specimen cross section. They interfere to produce moiré fringe patterns, representing the contour map of U or V displacement fields on the specimen grating. At each (x, y) point on the fringe pattern, the displacement can be calculated by [9]

$$U(x,y) = \frac{1}{2f_s}N_x(x,y) \quad V(x,y) = \frac{1}{2f_s}N_y(x,y) \qquad (1)$$

where N is the fringe order and f_s is the frequency of the specimen grating. In routine practice of moiré interferometry, $f_s = 1200$ lines/mm, which produces a contour interval of 417 nm per fringe order.

The real-time moiré interferometry setup described in [12] and [14] was used to document the thermal deformations of ECUs. A complete experimental setup is illustrated in Fig. 1. The major components in the setup include a portable engineering moiré interferometer and a computer-controlled environmental chamber. The required passive and active thermal loadings are provided by the convection oven, liquid nitrogen, and a power supply. A data acquisition (DAQ) hardware is used to record the temperatures of various locations of the specimen during experiments. With the setup, the in-plane deformations of ECUs can be documented as a function of temperature.

B. Silicon-Based Piezoresistive Stress Sensor

The sensor used in this paper is a complementary metal–oxide–semiconductor-based piezoresistive stress sensor [16]. Sensing elements are created by the channels of metal–oxide–semiconductor field-effect transistors (MOSFETs) in a current

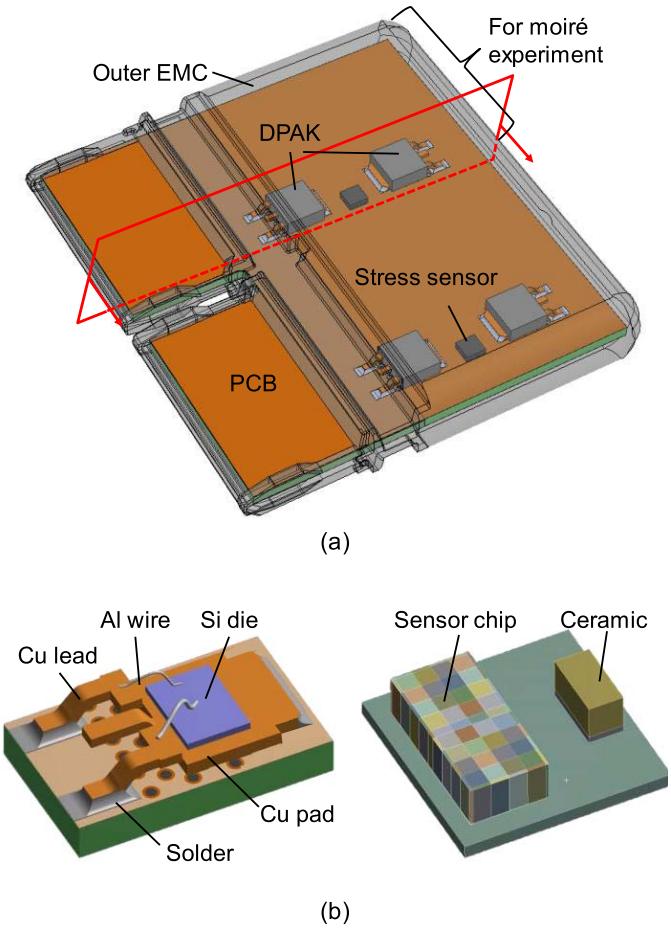

Fig. 3. Schematic illustration of (a) ECU test vehicle. (b) Internal details of the DPAK and the stress sensor.

mirror circuit on a silicon substrate [17]. The stress-sensitive channels of MOSFET in both branches of current mirrors are oriented differently with respect to the crystallographic axes of silicon, which makes the transistors respond differently to applied mechanical stresses. As a result, the circuit becomes out of balance under any mechanical stresses. This effect is quantified by measuring current differences in the two branches of the current mirror.

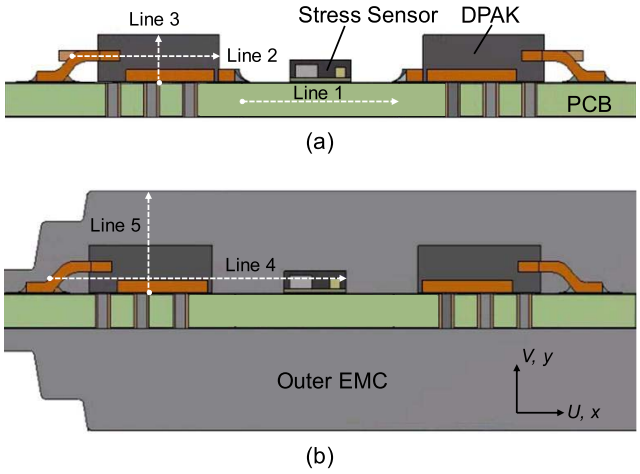

Fig. 4. Cross sections of moiré specimens (a) without and (b) with outer EMCs.

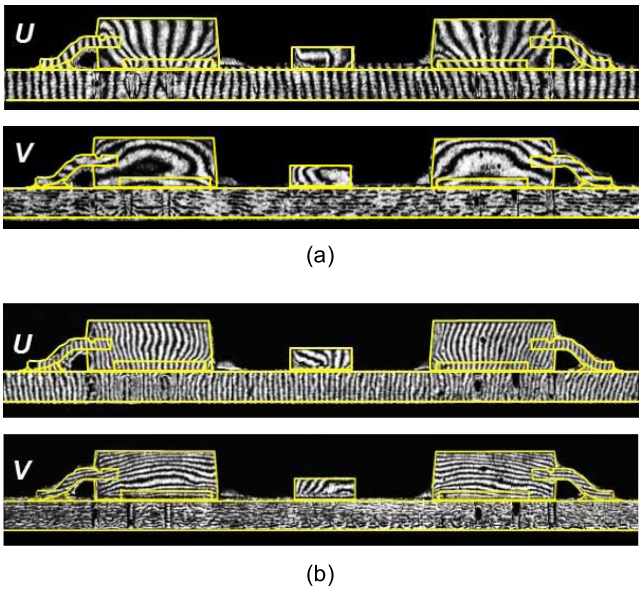

Fig. 5. Fringe patterns of unmolded ECU (a) at −40 °C and (b) at 125 °C.

In this paper, the p-channel metal–oxide–semiconductor (pMOS) current mirror with two channels in the directions of 0° and 90° is used for measurement of the in-plane normal stress difference. The applied stresses are determined from the measured current differences by

$$\sigma = \sigma_{xx} - \sigma_{yy} \approx -\frac{2}{\Pi_D^p(T)} \frac{I_D|_{0^\circ} - I_D|_{90^\circ}}{I_D|_{0^\circ} + I_D|_{90^\circ}} \tag{2}$$

where $\Pi_D^p(T)$ are the temperature-dependent effective piezoresistive constants that are influenced by the current mirror circuit for pMOS, I_D is the drain current of the current mirrors, and the subscripts indicate the directions of the channels.

The construction of the sensor used in this paper is shown in Fig. 2. The silicon chip consists of two stress sensors, and it is packaged in a standard land grid array (LGA) package [17]. Each stress sensor has 12 measurement cells, placed in 4×4 matrix (cells in the corners are inactive, left for bonding pads) [18].

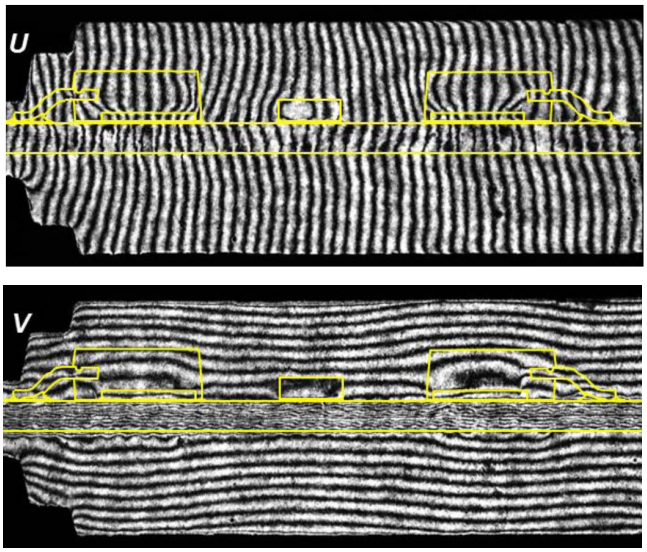

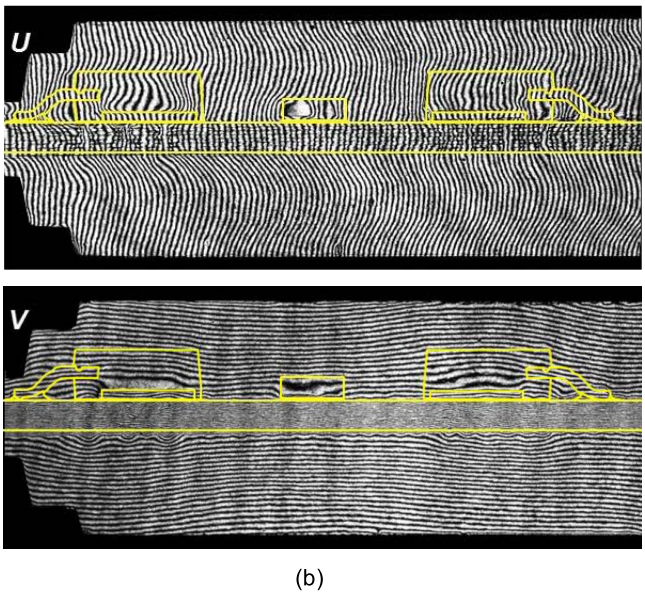

Fig. 6. Fringe patterns of molded ECU (a) at −40 °C and (b) at 125 °C.

III. Calibration and Validation of Numerical Model

A. Test Vehicle

A test vehicle used in this paper is shown schematically in Fig. 3(a). Two pairs of discrete packaging (DPAK) are mounted on a printed circuit board (PCB), and two stress sensors are mounted on the middle of each DPAK pair. The internal details of the DPAK and the stress sensor are shown in Fig. 3(b). The ECU was molded by an EMC through a transfer molding process. Two different specimens were used for displacement measurements: unmolded ECU (without outer EMC) and molded ECU (with outer EMC).

B. Displacement Measurements by Moiré Interferometry

The specimens were cut and ground flat to expose desired cross sections [see the red lines in Fig. 3(a)]. The cross sections

TABLE I
MATERIAL PROPERTIES OF NONPOLYMER MATERIALS

Material	Young's modulus [GPa]	Poisson's Ratio	CTE [ppm/°C]
Silicon die	x: 168.9 y: 168.9 z: 130.2	xy: 0.064 yz: 0.361 xz: 0.361	2.8
Copper in DPAK	125	0.34	17
Copper in PCB	80	0.34	17
Solder	49.55	0.36	20
Al wire	64	0.33	25.3
Ceramic	107	0.25	5

TABLE II
MATERIAL PROPERTIES OF POLYMER MATERIALS

Material	CTE [ppm/°C] bellow T_g	CTE [ppm/°C] above T_g	T_g [°C]
PCB prepreg	x: 14	x: 40	149
	y: 16	y: 40	
	z: 52	z: 247	
Outer EMC	12	25	110
DPAK mold	12	40	100
Sensor mold	8.2	26.7	106

of moiré specimens are shown in Fig. 4, where the DPAKs and the stress sensor are exposed on the cross sections. The cross-line diffraction gratings ($f_s = 1200$ lines/mm) were replicated on the cross sections.

The specimens were placed inside the convection oven, and the deformations were documented as a function of temperature from −40 °C to 125 °C. Fringe patterns recorded at −40 °C and 125 °C are shown in Figs. 5 and 6 for the package without and with outer mold, respectively, where the DPAK packages, the stress sensor, and the PCB were outlined directly on the fringe patterns. The displacement fields clearly show the complex nature of thermal deformations. It is worth noting that the deformations of DPAK packages in Fig. 6 are completely different from those in Fig. 5; it is attributed to the constraints from the outer EMC.

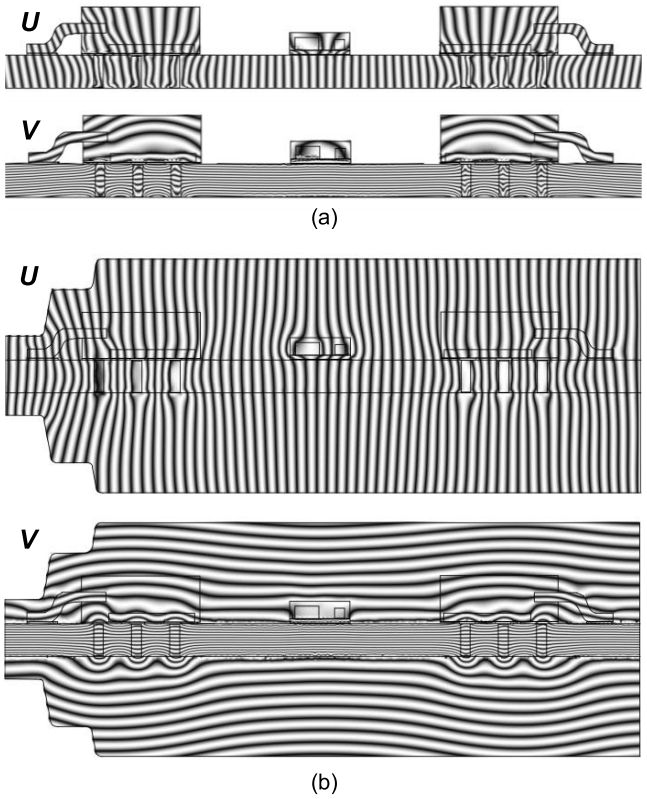

Fig. 7. Displacement fields at −40 °C obtained by FEA. (a) Unmolded ECU. (b) Molded ECU. The postprocessing produces the displacement fields with the same contour interval as the moiré fringes (417 nm).

C. Model Calibration

Detailed 3-D models with dimensions identical to the moiré specimens were constructed for model calibration. The material properties used in the numerical analysis are summarized in Tables I and II. A traction-free boundary condition was imposed on the cross sections to simulate the moiré experiments. The stress-free temperature was room temperature (22 °C), where the specimen grating was replicated. The same passive thermal loading used in the moiré experiment was applied to the models.

Representative displacement fields obtained at −40 °C are shown in Fig. 7 where the postprocessing produces the displacement fields with the same contour interval as the moiré fringes (417 nm). Quantitative comparisons between the modeling predictions and the moiré results are made in Figs. 8 and 9 for the unmolded and molded packages, respectively. The displacements were extracted from the fringe patterns in Figs. 5 and 6 first along the lines shown in Fig. 4. Then, the experimental results are compared with the initial modeling results in Figs. 8 and 9, which appear in the plots as "before calibration." The initial modeling predicted the deformation of PCB reasonably well, but a large discrepancy was observed in the DPAK and the outer EMC.

The outer EMC and DPAK mold occupy the majority of volume inside ECUs. They were calibrated to represent the effective properties that mimic the real behavior of the materials. A supplementary sensitivity study indicated that the deformation field was most sensitive to the coefficient of thermal expansion (CTE). The CTE values of these two materials were adjusted continuously until the discrepancy

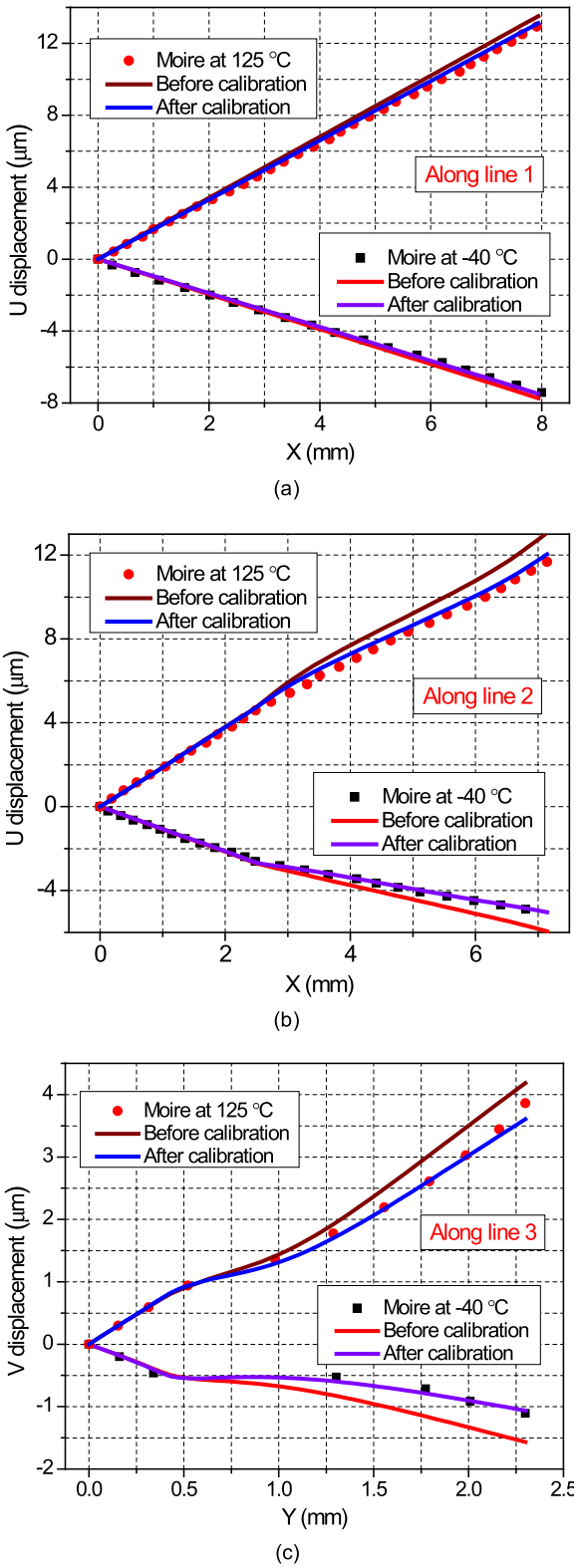

Fig. 8. Numerical predictions of the unmolded package subjected to a passive thermal loading condition are compared with experimental data shown in Fig. 5. (a) *U* along line 1 (PCB). (b) *U* along line 2 (DPAK). (c) *V* along line 3 (DPAK).

between numerical and experimental results became minimal. The CTE of the DPAK mold was calibrated first using experimental data of the unmolded ECU. The CTE of the outer EMC was subsequently calibrated using experimental data of

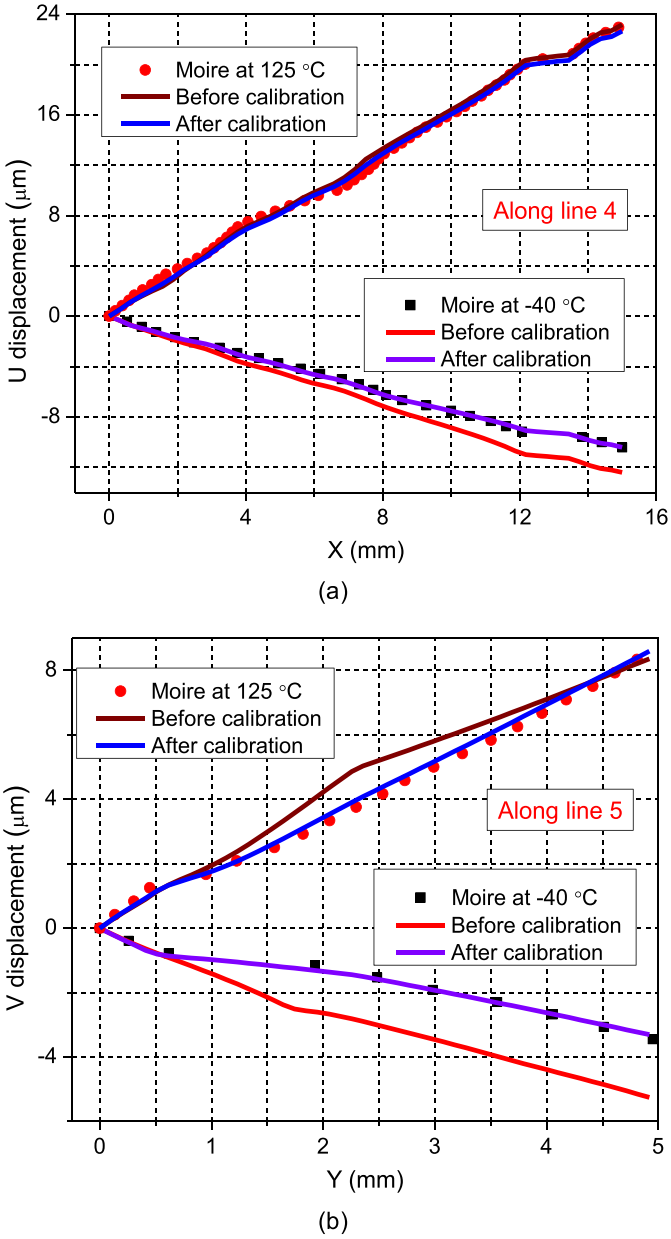

Fig. 9. Numerical predictions of the molded package subjected to a passive thermal loading condition are compared with experimental data shown in Fig. 6. (a) *U* along line 4. (b) *V* along line 5.

the molded ECU. The comparisons after calibration are also shown in Figs. 8 and 9 ("after calibration"). It is evident that the calibrated model can predict the displacement fields accurately.

D. Validation of Calibrated Model

A set of experiments under active thermal loading was conducted to verify the validity of the calibrated model. The specimen configuration had to be modified to utilize the DPAK power packages for active loading. The modification is shown in Fig. 10, where the power packages were placed slightly away from the stress sensor so that they were not damaged when the stress sensor was exposed to the cross section for moiré experiments.

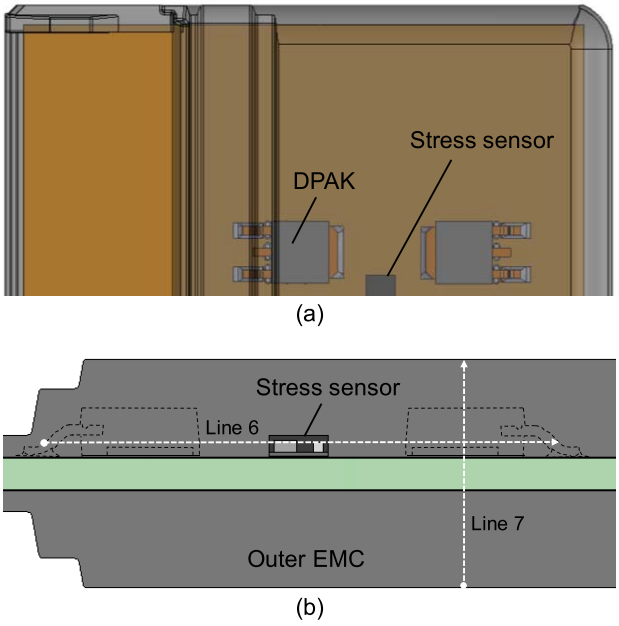

Fig. 10. Molded ECU specimen used for moiré experiments under active thermal loading. (a) Top view. (b) Front view.

Both DPAK packages were loaded by an electrical power of 1.2 W at room temperature (22 °C). The fringe patterns were recorded during the active loading. Representative fringe patterns obtained during the transient period are shown in Fig. 11(a), which were recorded at 260 s after DPAK packages were powered up. The fringe patterns in Fig. 11(b) were recorded at the thermal steady-state condition, which was obtained around 30 min after the power cycling started.

A thermal simulation was first conducted to obtain the temperature distribution at the steady-state condition. The surface temperatures at various locations at the steady-state condition were measured using thermocouples, and they were compared with the numerical predictions. The results are shown in Fig. 12, which corroborates the accuracy of the temperature prediction within ±3 °C.

The temperature distribution obtained from the thermal modeling was loaded to the calibrated structural model, and the deformation at the steady-state condition was calculated. The displacements were extracted along lines 6 and 7 [Fig. 10(b)] from the fringe patterns shown in Fig. 11(b), and they are compared with the numerical predictions in Fig. 13. The good correlations confirm the accuracy of the calibrated model.

IV. Implementation for Failure Prognostics

Several failure modes are known in the DPAK inside an ECU. They include delamination between molding compound and copper lead frame, wire bond failure, and solder joint failure [19]. Traditionally, the most dominant failure in the power electronic device happens at the bond wires and one of the most common failure modes is wire lift-off [20]–[22]. Fig. 14(a) shows an example of the interfacial delamination between the gate Al wire and Cu lead inside a molded ECU after a series of thermal cycling tests [2]. The interface between an aluminum wire bond and metal pad shown

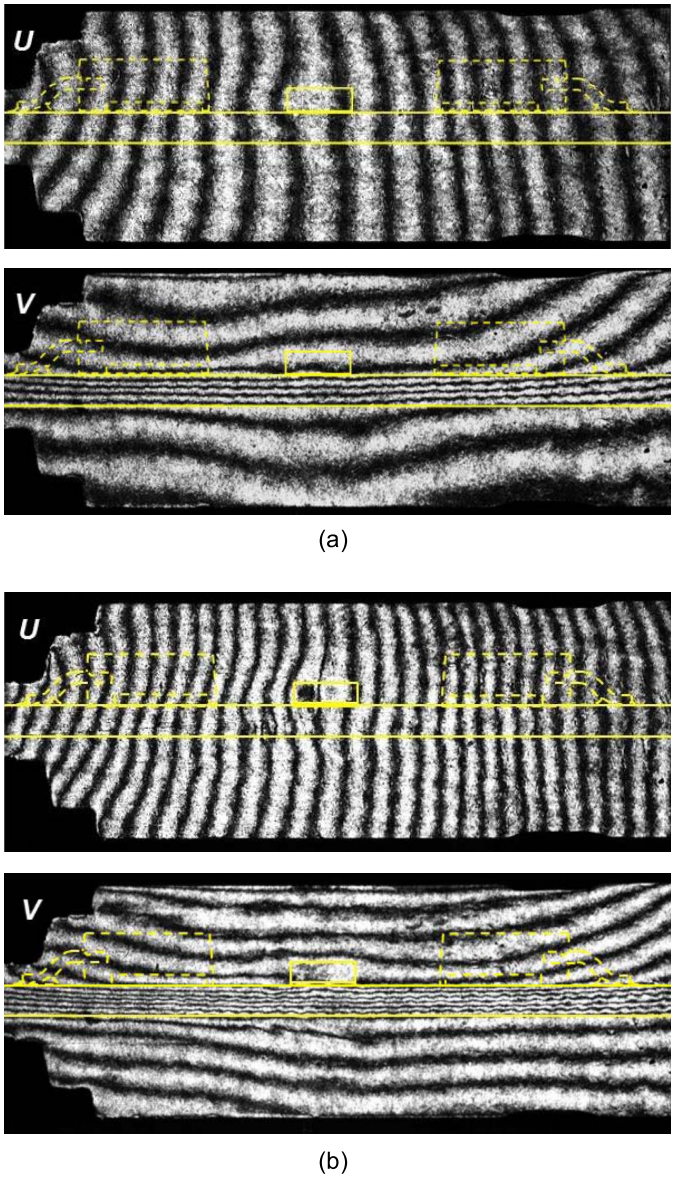

Fig. 11. Fringe patterns obtained (a) at 260 s after DPAK packages are powered up and (b) after the steady-state condition is reached.

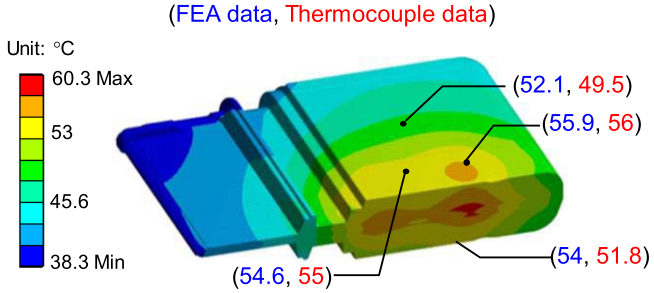

Fig. 12. Temperature distribution inside ECU at steady state.

in Fig. 14(b) is selected for the failure prognostics analysis in this paper.

A passive thermal cycling test is used to present the proposed method. The stress sensor is first used to count the actual operating conditions of five ECUs. Then, the calibrated FEA modeling is utilized to determine the thermally induced stresses of the wire bond of each unit.

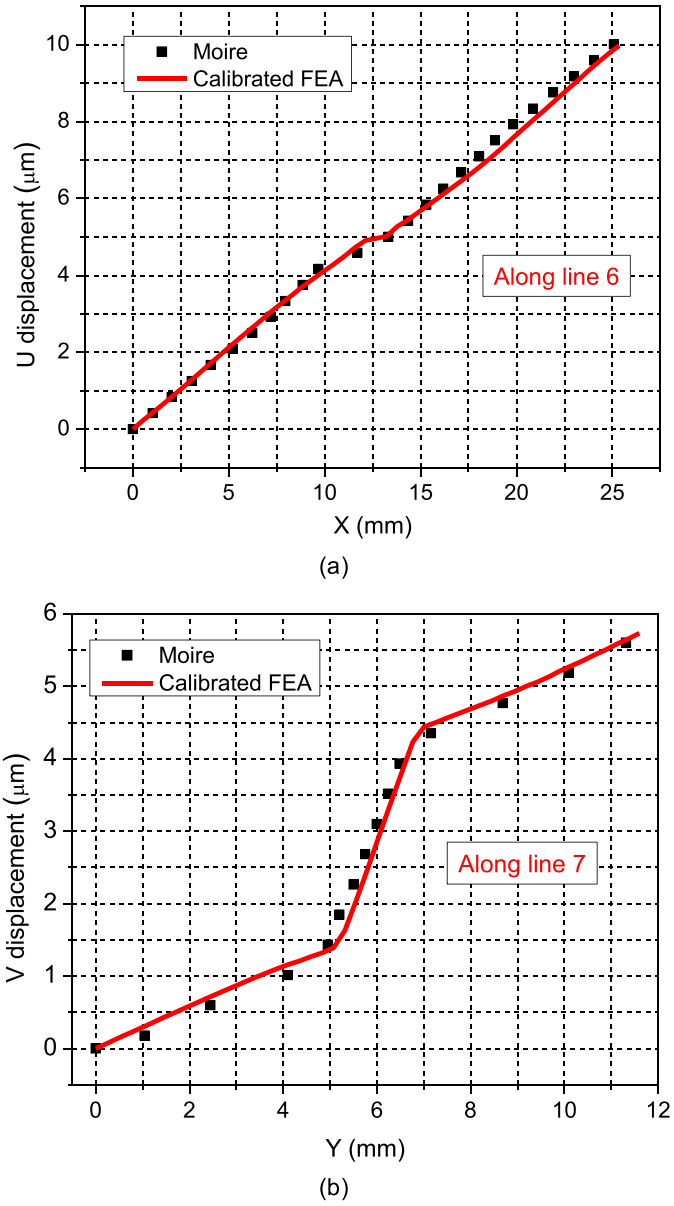

Fig. 13. Numerical predictions of the molded package subjected to an active thermal loading condition are compared with experimental data shown in Fig. 11. (a) U along line 6. (b) V along line 7.

A. Stress Prediction Using Calibrated Model

The calibrated FEA model of the molded ECU package used in the analysis is shown in Fig. 15(a), where the location of the stress sensor is marked by a red circle. Special considerations were given for the stress sensor cells. As can be seen from Fig. 15(b), the sensor was discretized to produce a 10-μm-thick top layer, which was equal to the thickness of the MOSFET branch in the stress sensor. In addition, each stress-sensing cell was divided into a 4×4 matrix of elements. Only the elements occupying the stress-sensitive current mirrors were used for stress calculations.

The FEA modeling was conducted to simulate the passive thermal loading of −40 °C–125 °C; the stress-free temperature was room temperature. The in-plane normal stress difference ($\sigma_{xx} - \sigma_{yy}$) was calculated from the elements representing the stress-sensing cells. The results at

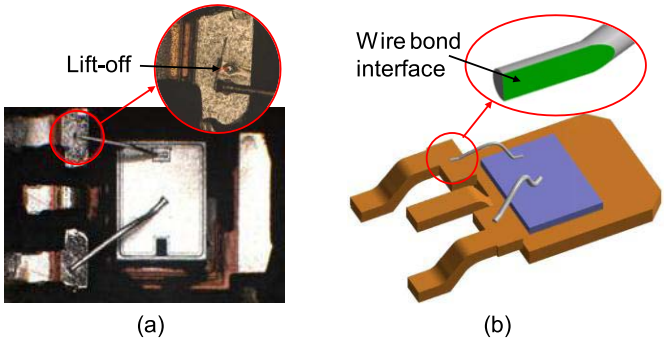

Fig. 14. (a) Wire bond "lift-off" failure in a DPAK. (b) Al wire bond interface of interest.

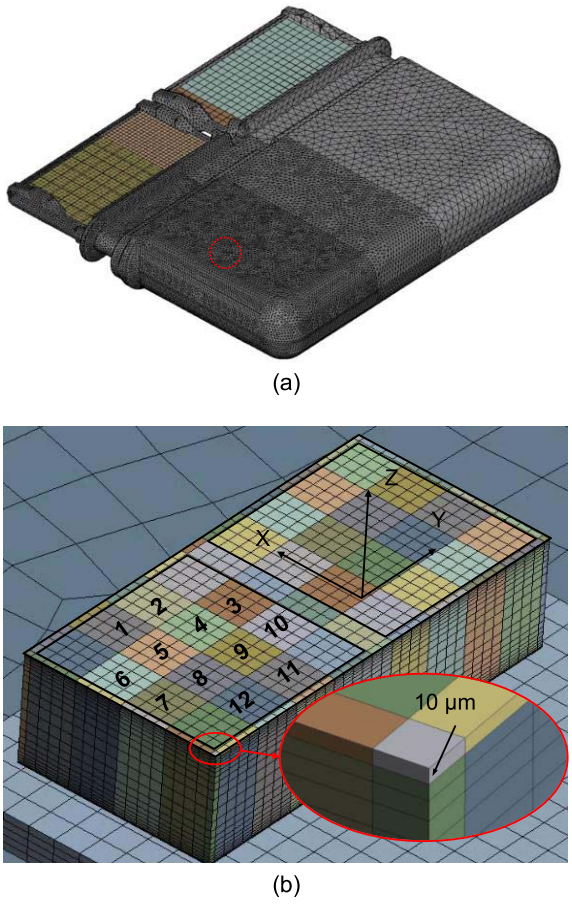

Fig. 15. FEA models of (a) whole ECU and (b) stress sensor.

−40 °C and 125 °C are plotted in Fig. 16(a) and (b), respectively.

The in-plane normal stress differences measured from an ECU that was subjected to the same thermal excursion are also plotted in Fig. 16. It is noted that the values were obtained by subtracting the stress signals at room temperature from those measured at −40 °C and 125 °C, which represented the in-plane normal stress differences caused by cooling or heating the unit to the two temperatures from room temperature. The comparison clearly indicates that the in-plane normal stress difference of each cell can be predicted by the calibrated FEA model quantitatively.

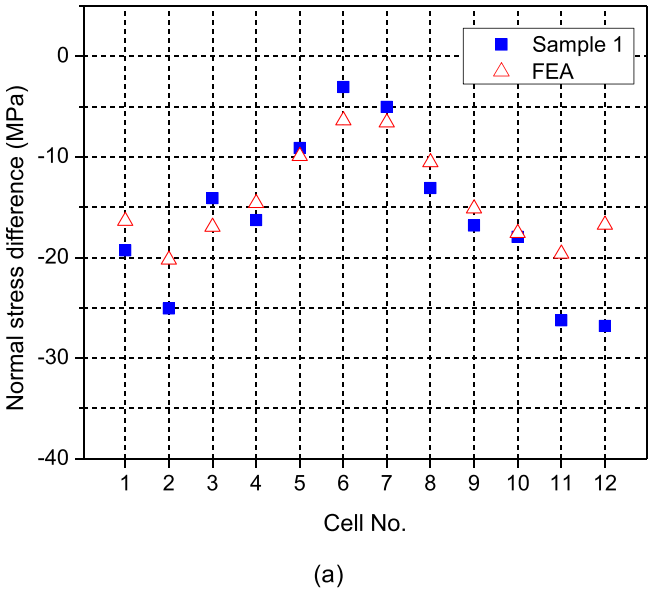

Fig. 16. Stress signals of an ECU is compared with the results obtained from FEA prediction (a) at −40 °C and (b) at 125 °C.

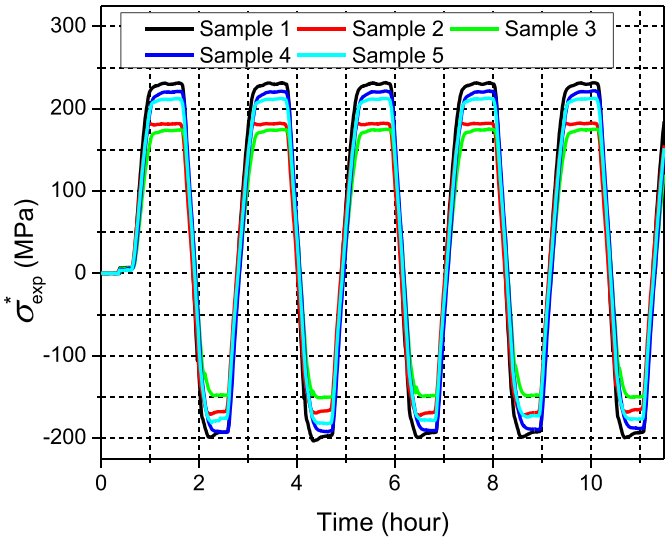

Fig. 17. Load-counter metric during the first five thermal cycles.

B. Stress Sensor as a Load Counter

The operating conditions of automotive vary significantly from locations to locations. The sensor can monitor the stress continuously, and it can be used to record the actual conditions under which an ECU is being operated (i.e., a load counter). The thermal cycling test and the calibrated model are employed to illustrate the load-counter concept.

A load-counter metric can be defined conceptually using the stress signals from all 12 cells as

$$\sigma^*(l) = \sum_{j=1}^{12} \sigma_j(l) = L(l) \tag{3}$$

where σ^* is a load-counter metric, σ_j is the value of in-plane normal stress difference from the jth cell, L is a load-counter function, and l is a load-counter variable that represents the *in situ* loading condition such as thermal loading, mechanical loading, and impact loading. The load-counter function can be obtained using the calibrated model when the load-counter variable is known. Then, the values of the load-counter variable $l(\sigma^*_{exp})$ corresponding to the *in situ* loading can be determined using the experimentally measured load-counter metric values σ^*_{exp} by the following inverse function:

$$l(\sigma^*_{exp}) = L^{-1}(\sigma^*_{exp}). \tag{4}$$

C. Implementation of Load-Counter for Passive Thermal Cycling

Five molded ECUs were placed in an environmental chamber and subjected to a passive thermal cycle of −40 °C to 125 °C. The stress data for each ECU were recorded during the test, from which the load-counter metric was calculated. The load-counter metric during the first five cycles is shown in Fig. 17. The large variations among the units are evident.

A relative large environmental chamber was used to accommodate all five ECUs as well as a large number of cables connecting the sensors to DAQ units. The temperature variation within the chamber was inevitable, which caused the large variations of stress signals among the units. Thus, the temperature variation was regarded as the load-counter variable in this paper.

In order to establish the load-counter function, the effect of the temperature variation on the stress-sensing cells was examined using the calibrated model. The representative stress signals around −40 °C and 125 °C are plotted in Fig. 18(a) and (b). The results clearly show that the stress signals from all 12 cells change consistently with the temperature variations. The load-counter metric was, then, calculated around −40 °C and 125 °C with a constant interval of 5 °C. The results are shown in Fig. 19. A linear function and a quadratic function were used to fit the results for the low- and high-temperature regions, respectively. The load-counter

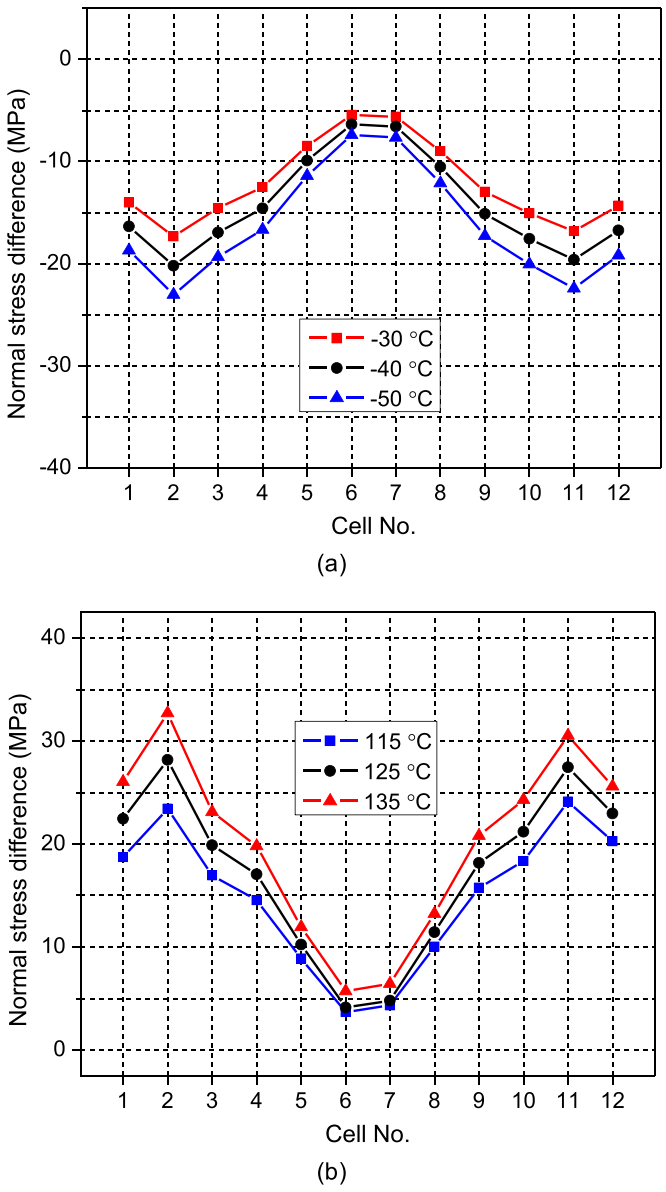

Fig. 18. Stress signals around (a) −40 °C and (b) 125 °C.

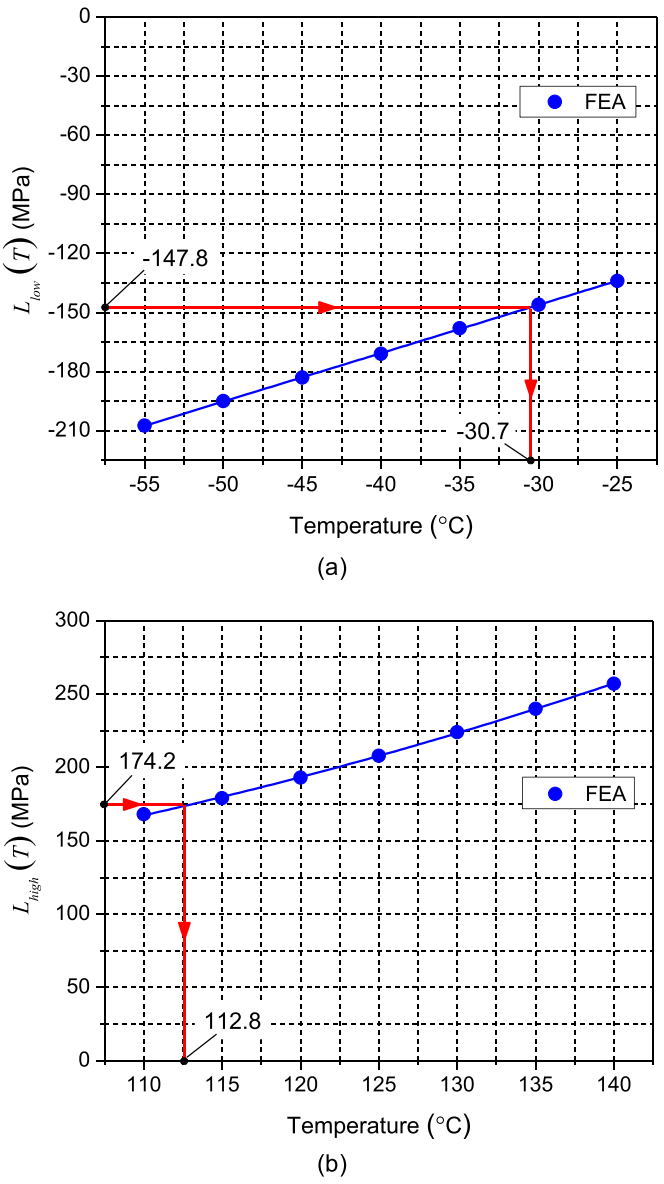

Fig. 19. Relationship between the load-counter metric and temperature at (a) low- and (b) high-temperature regions.

functions for two temperature regions are expressed as

$$\sigma^*_{\text{low}}(T) = L_{\text{low}}(T) = 2.45T - 72.57 \quad \text{for} \quad -55\ ^\circ\text{C} < T < -25\ ^\circ\text{C}$$
$$\sigma^*_{\text{high}}(T) = L_{\text{high}}(T) = 0.02T^2 - 2T + 145.36 \quad \text{for} \quad 110\ ^\circ\text{C} < T < 140\ ^\circ\text{C}. \tag{5}$$

Then, the *in situ* loading can be determined from the measured load-counter metric values using the above functions.

Fig. 19 illustrates how the *in situ* loading (T) was determined from the measured load-counter metric (σ^*_{exp}) using the value of Sample 3. At the low peak, the σ^*_{exp} value of Sample 3 was −147.8 MPa, which yielded the temperature loading of −30.7 °C. The corresponding values at the high peak were 174.2 MPa and 112.8 °C, respectively. The values of the load-counter metric measured from the units during the first thermal cycle, and the corresponding *in situ* loadings (T) are summarized in Table III. The *in situ* loading variation of the low-temperature (−40 °C) region is 18.4 °C, while the variation at the high-temperature (125 °C) region is 19.7 °C.

TABLE III
In Situ THERMAL LOADING DURING DWELL PERIODS

	Sample 1	Sample 2	Sample 3	Sample 4	Sample 5
At nominal -40 °C dwell period					
σ^*_{exp} [MPa]	-192.8	-167.7	-147.8	-192.9	-176.2
T (°C)	-49.0	-38.8	-30.7	-49.1	-42.3
At nominal 125 °C dwell period					
σ^*_{exp} [MPa]	231.5	181.8	174.2	220.9	212.1
T (°C)	132.5	115.8	112.8	129.1	126.4

The calibrated model used the *in situ* loadings to calculate the resultant forces acting on the interface between an aluminum wire bond and metal pad [see Fig. 14(b)]. The results are shown in Fig. 20(a) and (b) for the normal and shear forces, respectively. The difference of the forces at the wire

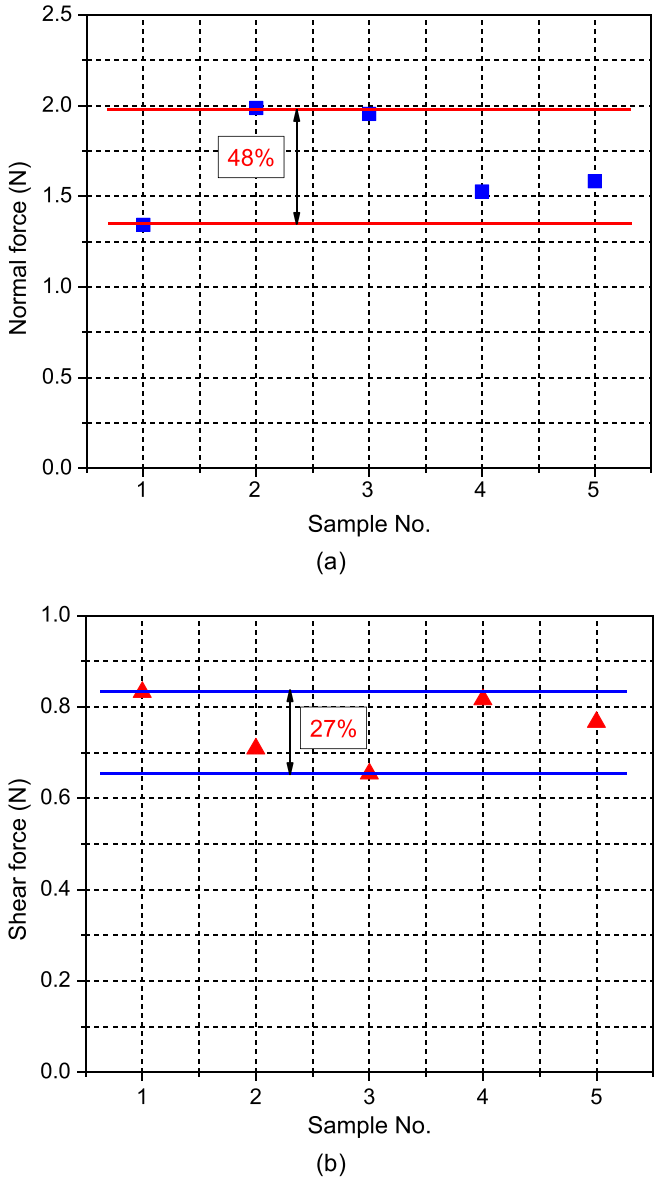

Fig. 20. Resultant forces acting on the Al wire bond interface. (a) Normal force. (b) Shear force.

bond interface among five units caused by the *in situ* loading variation is as large as 48% for the normal force and 27% for the shear force.

Large variations of the stress loading on the wire bond interface are evident, and thus different lifetimes are expected. The fatigue models can be utilized to predict the lifetime of wire bonds inside the DPAK under the thermal cyclic loading [21], [23]–[26]. Then, failure prognostics of the ECU product under the field condition can be performed using the damage index, such as the stress or strain range and the strain energy density, determined by the verified FEA model.

V. Conclusion

A model/sensor hybrid approach was developed and implemented for failure prognostics of an automotive ECU. In the approach, the predictability of a 3-D finite-element model for the complex molded ECU was calibrated and subsequently verified by moiré interferometry. The effective *in situ* loading history was obtained using the data obtained from a stress sensor in conjunction with a load-count metric that converted the stress signals into *in situ* temperature excursions. The calibrated model used the *in situ* loadings to calculate the resultant forces acting on the interface between an aluminum wire bond and metal pad. The significant differences were observed.

Although a relatively simple *in situ* thermal loading was used to illustrate the concept of the load-counter in this paper, the *in situ* stress sensor data could be converted for a wide range of *in situ* loadings. Then, the proposed hybrid approach can be used effectively to determine the actual loading variations of ECUs in the field, which can be subsequently utilized for failure prognostics.

References

[1] P. Gromala *et al.*, "Internal stress state measurements of the large molded electronic control units," in *Proc. 14th Int. Conf. Therm., Mech. Multi-Phys. Simulation Experim. Microelectron. Microsyst. (EuroSimE)*, Apr. 2013, pp. 1–8.

[2] D.-S. Kim, B. Han, A. Yadur, and P. J. Gromala, "Electronic control package model calibration using moiré interferometry," in *Proc. 15th Int. Conf. Therm., Mech. Multi-Phys. Simulation Experim. Microelectron. Microsyst. (EuroSimE)*, Apr. 2014, pp. 1–5.

[3] B. Wu, D.-S. Kim, B. Han, A. Palczynska, and P. J. Gromala, "Thermal deformation analysis of automotive electronic control units subjected to passive and active thermal conditions," in *Proc. 16th Int. Conf. Therm., Mech. Multi-Phys. Simulation Experim. Microelectron. Microsyst. (EuroSimE)*, Apr. 2015, pp. 1–6.

[4] Y. Chen, R. C. Jaeger, and J. C. Suhling, "CMOS sensor arrays for high resolution die stress mapping in packaged integrated circuits," *IEEE Sensors J.*, vol. 13, no. 6, pp. 2066–2076, Jun. 2013.

[5] M. Doelle, C. Peters, P. Ruther, and O. Paul, "Piezo-FET stress-sensor arrays for wire-bonding characterization," *J. Microelectromech. Syst.*, vol. 15, no. 1, pp. 120–130, Feb. 2006.

[6] P. Lall, M. N. Islam, M. K. Rahim, and J. C. Suhling, "Prognostics and health management of electronic packaging," *IEEE Trans. Compon. Packag. Technol.*, vol. 29, no. 3, pp. 666–677, Sep. 2006.

[7] B. Han and M. N. Variyam, "DMDTM package model calibration using interferometry," *Texas Instrum. Tech. J.*, pp. 1–9, 2001.

[8] Y. Guo, C. K. Lim, W. T. Chen, and C. G. Woychik, "Solder Ball Connect (SBC) assemblies under thermal loading: I. Deformation measurement via moiré interferometry, and its interpretation," *IBM J. Res. Develop.*, vol. 37, no. 5, pp. 635–648, Sep. 1993.

[9] D. Post, B. Han, and P. Ifju, *High Sensitivity Moiré: Experimental Analysis for Mechanics and Materials*. New York, NY, USA: Springer, 2012.

[10] B. Han and Y. Guo, "Determination of an effective coefficient of thermal expansion of electronic packaging components: A whole-field approach," *IEEE Trans. Compon., Packag., Manuf. Technol. A*, vol. 19, no. 2, pp. 240–247, Jun. 1996.

[11] B. Han, "Recent advancements of moiré and microscopic moiré interferometry for thermal deformation analyses of microelectronics devices," *Experim. Mech.*, vol. 38, no. 4, pp. 278–288, 1998.

[12] S. Cho, S. Cho, and B. Han, "Observing real-time thermal deformations in electronic packaging," *Experim. Techn.*, vol. 26, no. 3, pp. 25–29, 2002.

[13] B. Han, "Thermal stresses in microelectronics subassemblies: Quantitative characterization using photomechanics methods," *J. Therm. Stresses*, vol. 26, no. 6, pp. 583–613, 2003.

[14] S. Cho, B. Han, and J. Joo, "Temperature dependent deformation analysis of ceramic ball grid array package assembly under accelerated thermal cycling condition," *Trans. Amer. Soc. Mech. Eng. J. Electron. Packag.*, vol. 126, no. 1, pp. 41–47, 2004.

[15] P. G. Ifju and B. Han, "Recent applications of Moiré interferometry," *Experim. Mech.*, vol. 50, no. 8, pp. 1129–1147, 2010.

[16] A. P. Dorey, "A high sensitivity semiconductor strain sensitive circuit," *Solid-State Electron.*, vol. 18, no. 4, pp. 295–299, 1975.

[17] A. Palczynska, P. J. Gromala, D. Mayer, B. Han, and T. Melz, "*In-situ* investigation of EMC relaxation behavior using piezoresistive stress sensor," *Microelectron. Rel.*, vol. 62, pp. 58–62, Jul. 2016.
[18] A. Palczynska, A. Prisacaru, P. J. Gromala, B. Han, D. Mayer, and T. Melz, "Towards prognostics and health monitoring: The potential of fault detection by piezoresistive silicon stress sensor," *Microelectron. Rel.*, vol. 74, pp. 165–172, Jul. 2017.
[19] P. Gromala, A. Palczynska, and B. Han, "Prognostic approaches for the wirebond failure prediction in power semiconductors: A case study using DPAK package," in *Proc. 16th Int. Conf. Electron. Packag. Technol. (ICEPT)*, Aug. 2015, pp. 413–418.
[20] P. McCluskey, "Reliability of power electronics under thermal loading," in *Proc. 7th Int. Conf. Integr. Power Electron. Syst. (CIPS)*, Mar. 2012, pp. 1–8.
[21] L. Yang, P. A. Agyakwa, and C. M. Johnson, "Physics-of-failure lifetime prediction models for wire bond interconnects in power electronic modules," *IEEE Trans. Device Mater. Rel.*, vol. 13, no. 1, pp. 9–17, Mar. 2013.
[22] J. Onuki, M. Koizumi, and M. Suwa, "Reliability of thick Al wire bonds in IGBT modules for traction motor drives," *IEEE Trans. Adv. Packag.*, vol. 23, no. 1, pp. 108–112, Feb. 2000.
[23] J. M. Hu, M. Pecht, and A. Dasgupta, "A probabilistic approach for predicting thermal fatigue life of wire bonding in microelectronics," *J. Electron. Packag.*, vol. 113, no. 3, pp. 275–285, 1991.
[24] K. N. Meyyappan, P. Hansen, and P. McCluskey, "Wire fatigue models for power electronic modules," in *Proc. ASME Int. Mech. Eng. Congr. Expo.*, 2003, pp. 257–265.
[25] J. Bielen, J.-J. Gommans, and F. Theunis, "Prediction of high cycle fatigue in aluminum bond wires: A physics of failure approach combining experiments and multi-physics simulations," in *Proc. 7th Int. Conf. Thermal, Mech. Multiphys. Simulation Experim. Micro-Electron. Micro-Syst. (EuroSime)*, Apr. 2006, pp. 1–7.
[26] K. Sasaki *et al.*, "Thermal and structural simulation techniques for estimating fatigue life of an IGBT module," in *Proc. 20th Int. Symp. Power Semicond. Devices IC's (ISPSD)*, May 2008, pp. 181–184.

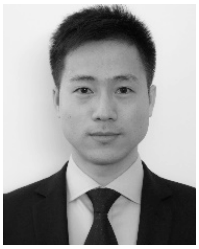

Bulong Wu received the B.S. and M.S. degrees in energy and power engineering from the Huazhong University of Science and Technology, Wuhan, China, in 2009 and 2012, respectively. He is currently pursuing the Ph.D. degree in mechanical engineering with the University of Maryland at College Park, College Park, MD, USA.

His current research interests include light-emitting diode, optomechanics, electronic packaging, and reliability.

Dae-Suk Kim received the B.S. and M.S. degrees in mechanical engineering from Pusan National University, Busan, South Korea, in 2008 and 2010, respectively, and the Ph.D. degree in mechanical engineering from the University of Maryland at College Park, College Park, MD, USA, in 2016.

He was a Post-Doctoral Research Associate with the Center for Advanced Life Cycle Engineering, University of Maryland at College Park. He is currently a Senior Engineer with Qualcomm Technologies, Inc., San Diego, CA, USA, where he is involved in thermomechanical finite-element modeling of solder joint life prediction, chip-package interaction, warpage prediction, material and design optimization, and material testing and characterization for mobile semiconductor packages. He has authored or co-authored one book chapter and over 20 journal and conference papers in the fields of microelectronics, higher power light-emitting diodes and laser diodes, and fuel cells. His current research interests include multiphysics computational mechanics, experimental mechanics for model validation and material characterization, design for reliability and manufacturing, and physics-of-failure-based prognostics of microelectronics.

Bongtae Han received the B.S. and M.S. degrees in mineral and petroleum engineering from Seoul National University, Seoul, South Korea, in 1981 and 1983, respectively, and the Ph.D. degree in engineering mechanics from Virginia Tech, Blacksburg, VA, USA, in 1991.

He is the Keystone Professor of engineering and the APT Chair of the Mechanical Engineering Department, University of Maryland at College Park, College Park, MD, USA. He is currently directing the Laboratory for Optomechanics and Micro/Nano Semiconductor/Photonics Systems, Center for Advanced Life Cycle Engineering, College Park. He has co-authored the textbook *High Sensitivity Moiré: Experimental Analysis for Mechanics and Materials* (Springer-Verlag, 1997) and edited two books. He has published 12 book chapters and over 250 journal and conference papers in the fields of microelectronics, photonics, and experimental mechanics. He holds two U.S. patents and four invention disclosures.

Dr. Han was elected as a fellow of the Society for Experimental Mechanics (SEM) and the American Society of Mechanical Engineering (ASME) in 2006 and 2007, respectively. He received the IBM Excellence Award for Outstanding Technical Achievements in 1994. He was a recipient of the 2002 SEM Brewer Award for his contributions to the development of photomechanics tools used in semiconductor packaging. He was a recipient of the 2016 ASME Mechanics Award at the Electronic and Photonic Packaging Division for his contributions to structural mechanics of electronic systems. His publication awards include the 2004 Best Paper Award of the IEEE TRANSACTIONS ON COMPONENTS AND PACKAGING TECHNOLOGIES, the Gold Award (Best Paper in the Analysis and Simulation Session) of the first Samsung Technical Conference in 2004, and the 2015 Best Paper Award of the 16th International Conference on Electronic Packaging Technology (ICEPT 2015). He served as an Associate Technical Editor for *Experimental Mechanics* from 1999 to 2001 and the *Journal of Electronic Packaging* from 2003 to 2012. He is currently serving as an Associate Editor for *Microelectronics Reliability*.

Alicja Palczynska, photograph and biography not available at the time of publication.

Alexandru Prisacaru received the master's degree in computational engineering from the Ruhr University of Bochum, Bochum, Germany, and the master's degree in structural engineering from Technical University Gheorghe Asachi, Iasi, Romania. He is currently pursuing the Ph.D. degree with Robert Bosch GmbH-Automotive Electronics, Reutlingen, Germany. His Ph.D. research is performed in cooperation with the Micro/Nanoelectronics System Integration and Reliability Department, Delft University of Technology, Delft, The Netherlands.

His current research interests include developing and implementing prognostics, health management techniques of relevant electronics for future autonomous driving applications, computational structural mechanics, material modeling, statistical pattern recognition, machine learning methods, and surrogate modeling.

Przemyslaw Jakub Gromala received the Ph.D. degree in mechanical engineering from the Cracow University of Technology, Krakow, Poland.

He was with the Delphi Development Center, Krakow, and the Infineon Research and Development Center, Dresden, Germany. He is a Simulation Senior Expert with Robert Bosch GmbH-Automotive Electronics, Reutlingen, Germany. He is currently leading an International Simulation Team and FEM Verification Lab with a main focus on implementation of simulation driven design for electronic control modules and multichip power packaging for hybrid drives. His current research interests include virtual prequalification techniques for development of the electronic control modules, multichip power packaging, material characterization and modeling, multidomain and multiscale simulation, including fracture mechanics, verification techniques, and prognostics, and health monitoring for future safety-related electronic smart systems.

Dr. Gromala is an Active Committee Member of the IEEE conferences: Electronic Components and Technology Conference, Thermal and Mechanical Simulation and Experiments in Microelectronics and Microsystems, International Conference on Electronic Packaging Technology, American Society of Mechanical Engineers: InterPACK. He is an Active Committee Member of the European Technology Platform on Smart Systems Integration, defining research and development and innovation needs as well as policy requirements related to smart systems integration and integrated micro- and nano-systems.